Modeling of magnetization characteristics and faster magnetodynamic field computation (invited)

Y. Saito, Y. Kishino, K. Fukushima, S. Hayano, and N. Tsuya
College of Engineering, Hosei University, 3-7-2 Kajinocho Koganei, Tokyo 184, Japan

A Chua-type magnetization model is derived by means of a Fourier series while the magnetic flux density is sinusoidally varying with time. It is shown that this Chua-type model is well suited for practical computations of magnetodynamic field. A geometrical duality between the Delaunay triangles and associated Voronoi polygons is utilized to implement a dual energy finite element approach. As an example, the magnetodynamic fields in a toroidal reactor including the effects of transients, eddy currents, and hysteresis are computed.

I. INTRODUCTION

Modeling of magnetization characteristics of the magnetic materials is of paramount importance for magnetic field computations in electromagnetic devices. In the present paper, we derive a Chua-type magnetization model by means of a Fourier series, and show that this Chua-type model is well suited for practical computations of the magnetodynamic field in electrical machines.[1] Also, it is clarified that this Chua-type model is closely related to the Preisach- and Rayleigh-type models.

In order to evaluate the magnetodynamic fields in the most efficient manner, a geometrical duality between the Delaunay triangles and associated Voronoi polygons is utilized to implement a dual energy finite element approach.[2,3] This new approach requires the use of a single potential to establish the upper and lower bounds of solutions in electromagnetic field problems, whereas the conventional dual energy finite element approach requires the use of two different types of potentials (vector and scalar).

As an example, the magnetodynamic fields in a toroidal reactor including the effects of transients, eddy currents, and hysteresis are computed. It is shown by comparison with experiment that our procedure models the sinusoidal response and hysteresis loops with a high degree of precision. Also, we find that our new dual energy approach yields the solutions in 1/50 of the computation time required for the traditional first-order finite element method.

II. MAGNETIZATION MODEL

A. Chua-type model

When flux density B is sinusoidally varying with time t, then the associated field intensity H becomes a nonsinusoidal periodic wave. Figure 1(a) shows a B-H loop, and Fig. 1(b) shows the wave forms of B and H. By means of a Fourier series, the field intensity H in Fig. 1(b) is expanded into the sine and cosine series, that is,

$$H = \sum_{n=1}^{\infty} H_{sn} \sin(n\omega t) + \sum_{n=1}^{\infty} H_{cn} \cos(n\omega t), \quad (1)$$

where ω denotes the angular velocity of B. Let T be the period of B, then $\omega = (2\pi/T)$, and the Fourier coefficients H_{sn}, H_{cn} for nth harmonics are given by

$$H_{sn} = \frac{2}{T}\int_0^T H \sin(n\omega t)\,dt, \quad (2)$$

$$H_{cn} = \frac{2}{T}\int_0^T H \cos(n\omega t)\,dt. \quad (3)$$

The odd and even components of H are respectively obtained by

$$H_o = \sum_{n=1}^{\infty} H_{sn} \sin(n\omega t), \quad (4)$$

$$H_e = \sum_{n=1}^{\infty} H_{cn} \cos(n\omega t). \quad (5)$$

As shown in Figs. 1(c) and 1(d), the odd component H_o and even component H_e are respectively in phase with the flux density B and the time derivative of flux density dB/dt. Thereby, a combination of H_o with B yields one of the

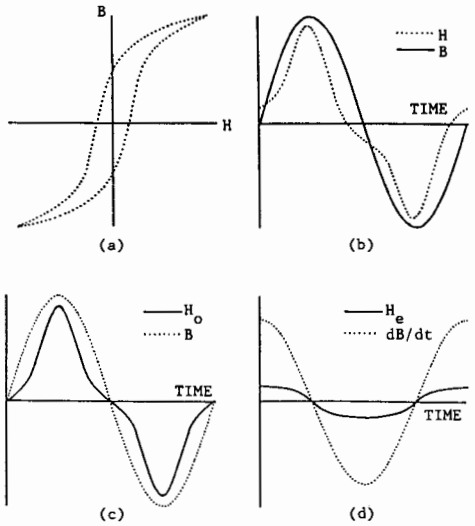

FIG. 1. (a) B-H loop; (b) time variations of B and H; (c) B and odd component H_0 of H; and (d) dB/dt and even component H_e of H.

 0021-8979/88/083174-05$02.40

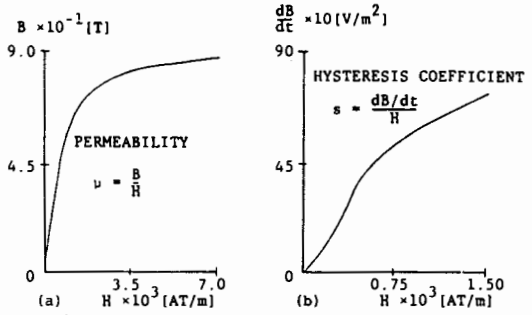

FIG. 2. (a) B-H_0 curve which represents the saturation property and (b) dB/dt-H_e curve which represents the hysteretic property.

saturation curves. Also, a combination of H_e with dB/dt yields a curve which represents the hysteretic property, because $H_e(dB/dt)$ provides the power loss per unit volume. Figures 2(a) and 2(b) show the practical examples of B-H_o and dB/dt-H_e curves, respectively. In other words, by considering the relations of Figs. 2(a) and 2(b), it is possible to write the field intensity H as

$$H = H_o + H_e = f_s(B) + f_h(dB/dt)\,, \tag{6}$$

where $f_s(B)$ and $f_h(dB/dt)$ are denoting the single valued functions of B and dB/dt, respectively. This means that the saturation property is a function of the flux density B only, and the hysteretic property is a function of the time derivative of flux density dB/dt only.

By defining the permeability μ and hysteresis coefficient s as

$$\mu = B/H_o, \tag{7}$$

$$s = (dB/dt)/H_e, \tag{8}$$

relation (6) is expressed by

$$H = (1/\mu)B + (1/s)dB/dt\,. \tag{9}$$

Equation (9) is obviously one of the Chua-type models.

B. Preisach-type model

According to Ref. 4, the reversing point field intensity H_n and applied field intensity H_p are defined as shown in Fig. 3. By considering Fig. 3, it is obvious that the B-vs-H trajectory takes different paths depending on the reversing point field intensity H_n. Thereby, the flux density B is represented as a function of the applied field intensity H_p as well as reversing point field intensity H_n, viz.,

$$B = B(H_p, H_n)\,. \tag{10}$$

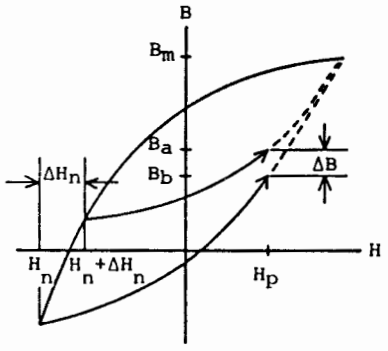

FIG. 3. Derivation of Preisach's function Ψ.

Moreover, by considering a saturation point of flux density on the nonsymmetrical hysteresis loop shown in Fig. 3, it is revealed that the B-vs-H trajectories take different paths according to the reversing point of field intensities but always coincide at the saturation point of flux density. Therefore, the rate of change of slope $\partial B/\partial H_p$ with the reversing point field intensity H_n takes nonzero values in the region $|B| < B_m$, where B_m is the saturation flux density. This relationship gives the definition of Preisach's function ψ as

$$\psi = \frac{\partial^2 B(H_p, H_n)}{\partial H_n \partial H_p}\,. \tag{11}$$

When we apply Eq. (11) to a lower branch of a Rayleigh loop,[5]

$$B = (\mu_i + \nu H_n)H_p + (\nu/2)(H_p^2 - H_n^2)\,, \tag{12}$$

then it is possible to obtain the following relationship:

$$\psi = \nu, \tag{13}$$

where ν, μ_i are, respectively, the Rayleigh's constant and initial permeability. Thus, it is obvious that the Rayleigh's model is one of the Preisach-type models.

C. Comparison of models

The Chua-type model is based on the fact that the magnetization path is uniquely determined by $\partial B/\partial t$. On the other hand, the Preisach-type model is based on a behavior that the change of slope $\partial B/\partial H$ depends on the reversing point field intensities.

In order to find a relationship between them, application of Eq. (9) to the states of Fig. 3 gives the following relations:

$$H_p = (1/\mu)B_a + (1/s)\frac{\partial B_a}{\partial t}\,, \tag{14}$$

$$H_p = (1/\mu)B_b + (1/s)\frac{\partial B_b}{\partial t}\,, \tag{15}$$

where the field intensity ΔH_n in Fig. 3 is so small that the permeability μ and hysteresis coefficient s may be assumed to be constant. By subtracting Eq. (14) from Eq. (15) and rearranging, it is possible to obtain

$$\Delta B/\mu = (1/\mu)(B_a - B_b) = (1/s)\left[\left(\frac{\partial B_b}{\partial t}\right) - \left(\frac{\partial B_a}{\partial t}\right)\right]$$
$$= (1/s)\left[\left(\frac{\partial B_b}{\partial H_p} - \frac{\partial B_a}{\partial H_p}\right)\frac{\partial H_p}{\partial t}\right]. \tag{16}$$

Further rearrangement of Eq. (16) yields

$$s\Big/\left(\frac{\partial H_p}{\partial t}\right) = (\mu/\Delta B)\left[\left(\frac{\partial B_b}{\partial H_p}\right) - \left(\frac{\partial B_a}{\partial H_p}\right)\right]. \tag{17}$$

In Fig. 3, if the limit of ΔH_n goes to zero, then the $\Delta B/\mu$ term in Eq. (17) is simultaneously reduced to zero. Thus an assumption of $\Delta H_n = \Delta B/\mu$ leads to

$$\lim_{\Delta H_n \to 0} (\mu/\Delta B)\left[\left(\frac{\partial B_b}{\partial H_p}\right) - \left(\frac{\partial B_a}{\partial H_p}\right)\right] = \frac{\partial^2 B}{\partial H_n \partial H_p}\,. \tag{18}$$

From Eqs. (11), (17), and (18), a relationship between the hysteresis coefficient s and the Preisach's function ψ is obtained as

$$s=\psi\left(\frac{\partial H}{\partial t}\right). \tag{19}$$

III. FASTER MAGNETODYNAMIC FIELD COMPUTATION

A. Basic equations

Consider the cross section of a toroidal reactor shown in Fig. 4. The governing equations for the electric and magnetic fields in the system are

$$\nabla\times E=-\frac{\partial B}{\partial t}, \tag{20}$$

$$\nabla\times H=J, \tag{21}$$

$$E=\rho J, \tag{22}$$

where $E, J,$ and ρ are, respectively, the electric field intensity, current density, and resistivity. Combining Eqs. (20)–(22) yields

$$\rho\nabla\times\nabla\times H=-\frac{\partial B}{\partial t}. \tag{23}$$

Furthermore, only the axial component of the magnetic field exists, so that Eq. (23) is simplified to

$$\rho\frac{\partial^2 H}{\partial x^2}+\rho\frac{\partial^2 H}{\partial y^2}=\frac{\partial B}{\partial t}, \tag{24}$$

where the magnetic field intensity H and flux density B are related by Eq. (9).

B. Locally orthogonal discretization

A method of locally orthogonal discretization is presented in Refs. 2 and 3. The key concept in this procedure is to exploit the geometric duality that exists between Delaunay triangles and Voronoi polygons. Delaunay triangles and Voronoi polygons are related by the fact that vertices of the Voronoi polygons are the circumcenters of the Delaunay triangles.[6] As explained in Ref. 3 and illustrated in Fig. 5, one of the features of this Voronoi–Delaunay duality is that the sides of the Voronoi polygons are perpendicular to the sides of the Delaunay triangles. This relationship leads to a locally orthogonal coordinate system as shown in Fig. 5. When the vertices i, j of the Delaunay triangle and the vertices k, l of the Voronoi polygon are chosen as node points,

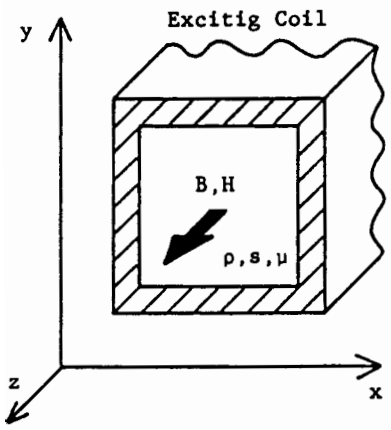

FIG. 4. Cross section of a toroidal reactor.

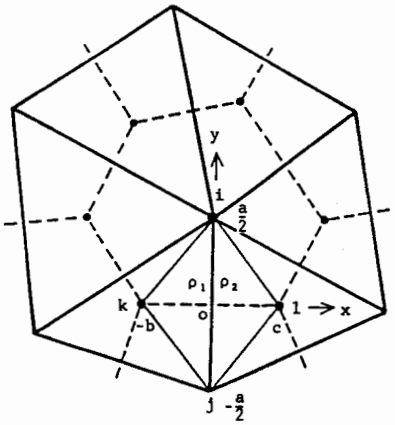

FIG. 5. Voronoi–Delaunay diagram showing the locally orthogonal coordinate system.

the trial functions are independently defined along the x and y axis.[3] Thus, the governing Eq. (24) is divided into x and y components, that is,

$$\rho\left(\frac{\partial^2 H}{\partial x^2}\right)=\left(\frac{1}{2}\right)\left(\frac{\partial B}{\partial t}\right), \tag{25}$$

$$\rho\left(\frac{\partial^2 H}{\partial y^2}\right)=\left(\frac{1}{2}\right)\left(\frac{\partial B}{\partial t}\right). \tag{26}$$

C. Functional and node equations

Current density in the x and y directions is given by

$$J_x=\left(\frac{\partial H}{\partial y}\right), \tag{27}$$

$$J_y=-\left(\frac{\partial H}{\partial x}\right). \tag{28}$$

As shown in Fig. 5, the resistivity ρ has a different value in each Delaunay triangle. At the interface between regions of the different resistivity ρ, the normal component of current density to the boundary must be continuous. This condition is satisfied by selecting a trial function for the y direction as

$$H_p=(\tfrac{1}{2})(H_i+H_j)+(H_i-H_j)(y/a), \tag{29}$$

where the length a in the direction of the y axis shown in Fig. 5. Substituting Eq. (29) into Eq. (27) shows that the current density J_x is continuous at the boundary with this approximation.

The other boundary conditions to be satisfied is that the tangential component of electric field intensity at the boundary must be common to both regions. This condition is satisfied by the following trial functions in the x direction:

$$\begin{aligned}H_c=&[(\rho_1/b)H_k+(\rho_2/c)H_l]/[(\rho_1/b)+(\rho_2/c)]\\&+(H_l-H_k)(\rho_2 x/bc)/[(\rho_1/b)+(\rho_2/c)],\\&-b\leqslant x\leqslant 0,\end{aligned} \tag{30}$$

$$\begin{aligned}H_c=&[(\rho_1/b)H_k+(\rho_2/c)H_l]/[(\rho_1/b)+(\rho_2/c)]\\&+(H_l-H_k)(\rho_1 x/bc)/[(\rho_1/b)+(\rho_2/c)],\\&0\leqslant x\leqslant c,\end{aligned} \tag{31}$$

where the lengths b,c in the direction of the x axis are shown in Fig. 5. Substituting Eqs. (30) and (31) into Eq. (28) reveals the $E_y=\rho_1 J_y=\rho_2 J_y$ is satisfied at the boundary. Since the Delaunay system obeys the boundary condition

corresponding to continuity of the current density, a functional for the Delaunay system is

$$F=\int_{-a/2}^{a/2}\int_{c}^{-b}\left[\rho(J_x)^2-H_p\left(\frac{\partial B}{\partial t}\right)\right]dx\,dy\,. \tag{32}$$

On the other hand, the Voronoi system obeys the boundary condition of electric field intensity $E_y=\rho J_y$, and this yields the following functional for the Voronoi systems

$$G=-\int_{-a/2}^{a/2}\int_{-b}^{c}\left[(1/\rho)(E_y)^2-\hat{H}_c\left(\frac{\partial B}{\partial t}\right)\right]dx\,dy\,, \tag{33}$$

where $\hat{}$ denotes the prescribed value.

By means of Eqs. (27)–(33), it is possible to obtain the following nodal equations:

$$\left(\frac{\partial F}{\partial H_j}\right)=[(b\rho_1/a)+(c\rho_2/a)](H_j-H_i)+\left(\frac{\partial\phi_{jl}}{\partial t}\right)=0\,, \tag{34}$$

$$\left(\frac{\partial G}{\partial H_k}\right)=(H_k-H_l)/[(b/a\rho_1)+(c/a\rho_2)]+\left(\frac{\partial\phi_{kl}}{\partial t}\right)=0\,, \tag{35}$$

where

$$\phi_{jl}=\int_{-a/2}^{0}\int_{-b}^{c}B\,dx\,dy,\quad \phi_{kl}=\int_{-a/2}^{a/2}\int_{-b}^{0}B\,dx\,dy\,.$$

Equations (34) and (35) are the equations corresponding to the node j of the Delaunay system and to the node k of the Voronoi system, respectively.

D. Electric circuits

With Δz denoting the length of the magnetic flux path, Eqs. (34) and (35) can be rewritten as

$$(r_{bp}+r_{cp})(i_j-i_i)+\left(\frac{\partial\phi_{jl}}{\partial t}\right)=0\,, \tag{36}$$

$$(i_k-i_l)/[(1/r_{bc})+(1/r_{cc})]+\left(\frac{\partial\phi_{kl}}{\partial t}\right)=0\,, \tag{37}$$

where

$$i_i=H_i\Delta z,\quad i_j=H_j\Delta z,\quad i_k=H_k\Delta z,\quad i_l=H_l\Delta z,$$
$$r_{bp}=\rho_1 b/(a\Delta z),\quad r_{cp}=\rho_2 c/(a\Delta z),$$
$$r_{bc}=\rho_1 a/(b\Delta z),\quad r_{cc}=\rho_2 a/(c\Delta z)\,. \tag{38}$$

Let ϕ_j and ϕ_k denote the magnetic fluxes passing through the Voronoi polygon centered at node j and the Delaunay triangle centered at node k. The electric circuits for Delaunay and Voronoi systems are shown in Figs. 6(a) and 6(b), respectively.

E. Magnetic circuits

With ΔS_j denoting the area of the Voronoi polygon, the magnetic circuit equation for node j is derived from Eq. (9) as

$$i_j+ni_e=M_j\phi_j+N_j\left(\frac{\partial\phi_j}{\partial t}\right), \tag{39}$$

where

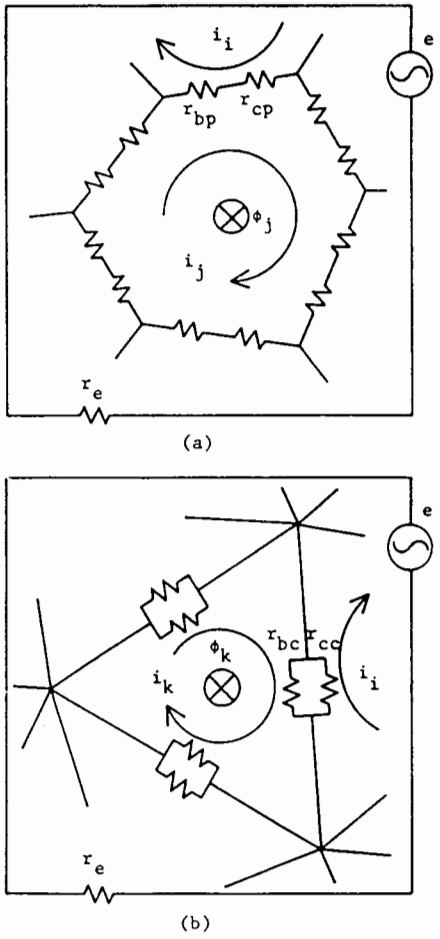

FIG. 6. (a) Electric circuit for eddy currents in the Delaunay system and (b) electric circuit for eddy currents in the Voronoi system.

$$M_j=\Delta z/(\mu\Delta S_j),\quad N_j=\Delta z/(s\Delta S_j)\,, \tag{40}$$

and n, i_e are the number of turns of the exciting coil and the exciting current, respectively.

Similary, a magnetic circuit equation for node k is derived as

$$i_k+ni_e=M_k\phi_k+N_k\left(\frac{\partial\phi_k}{\partial t}\right), \tag{41}$$

where

$$M_k=\Delta z/(\mu\Delta S_k),\quad N_k=\Delta z/(s\Delta S_k)\,, \tag{42}$$

and ΔS_k is the area of the Delaunay triangle.

F. Time discretization

The full Voronoi and Delaunay systems are best expressed in matrix notation as

$$RI+W\left(\frac{d}{dt}\right)\Phi=V, \tag{43}$$

where R, W, V, I, Φ are the resistance matrix, winding matrix, voltage vector, current, and flux vector, respectively. Also, magnetic circuit system equations are expressed as

$$W^TI=M\Phi+N(d/dt)\Phi\,, \tag{44}$$

where a superscript T denotes the transpose of matrix. By

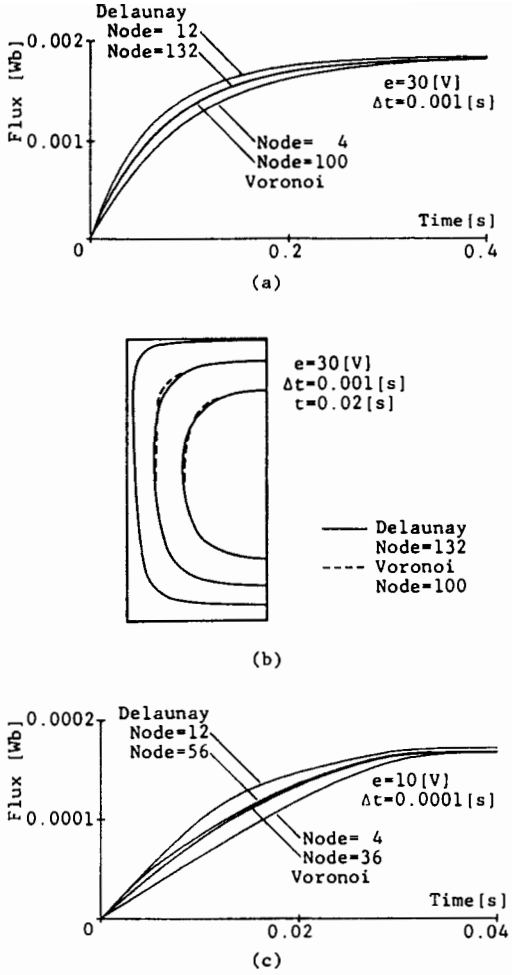

FIG. 7. (a) Step response of a toroidal reactor assuming linear permeability and hysteresis coefficient s; (b) computed magnetic flux density distributions for a step input assuming the linear permeability and hysteresis coefficient s; and (c) step response for the reactor taking the saturation of iron into account but neglecting hysteresis.

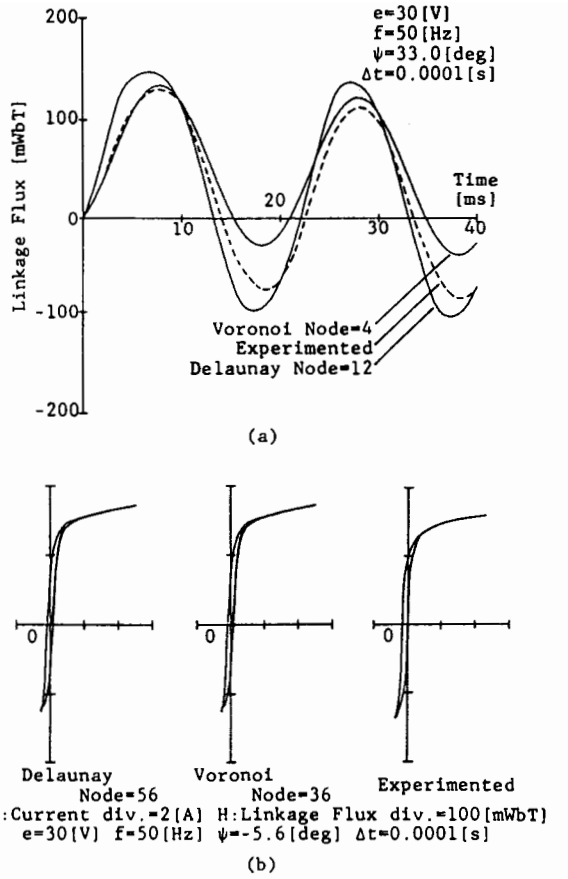

FIG. 8. (a) Sinusoidal response together with experimental results and (b) computed and experimental dynamic hysteresis loops for the laminated toroidal core.

means of Eqs. (43) and (44), a system of dynamic magnetic field equations is reduced to the following form:

$$W^T G V = M\Phi + (W^T G W + N)(d/dt)\Phi\,, \tag{45}$$

where the conductance matrix G is the inverse matrix of the resistance matrix R. Equation (45) is discretized in time t by using the following process

$$\begin{aligned} W^T G V_{t+(\Delta t/2)} &= M_{t+(\Delta t/2)}(\tfrac{1}{2})(\Phi_{t+\Delta t} + \Phi_t) \\ &\quad + (W^T G W + N_{t+(\Delta t/2)})(1/\Delta t) \\ &\quad \times (\Phi_{t+\Delta t} - \Phi_t)\,, \end{aligned} \tag{46}$$

where the subscripts $t, t+(\Delta t/2), t+\Delta t$ denote the corresponding times and Δt denotes the stepwidth in time. It must be noted that because of Eq. (6) the elements in magnetic resistance matrix M and hysteresis parameter matrix N in Eq. (46) are generally nonlinear functions of the flux and time derivative of flux. The field solution thus takes these nonlinearities into account.

IV. RESULTS AND CONCLUDING REMARKS

Various constants used in the computation are given in Refs. 1 and 2, and the magnetization curves for permeability and for hysteresis coefficient are given by Figs. 2(a) and 2(b). Figure 7(a) shows the step response of the toroidal reactor assuming linear permeability and hysteresis coefficient and Fig. 7(b) shows the computed flux density distributions. Figure 7(c) shows the step response taking into account the saturation of the iron but neglecting its hysteresis. It is found that the average value of the Delaunay and the Voronoi solutions yields excellent results even with a small number of nodes employed. Figure 8(a) shows the sinusoidal response of the toroid together with experimental measurements. Figure 8(b) shows the computed and measured dynamic hysteresis loops for the laminated toroidal core; this comparison demonstrates the validity of the hysteresis model.

As shown above, it is possible to calculate dynamic magnetic fields in an efficient manner using a new method based on the geometrical duality of Delaunay triangles and Voronoi polygons. We have shown by example that the new method is 50 times as efficient as the conventional first-order finite element method.

[1] Y. Saito, IEEE Trans. Magn. **MAG-18**, 546 (1982).
[2] Y. Saito, S. Hayano, and N. Tsuya, *et al.*, IEEE Trans. Magn. **MAG-21**, 2280 (1985).
[3] Y. Saito, Y. Kishino, S. Hayano, H. Nakamura, N. Tsuya, and Z. J. Cendes, *et al.*, IEEE Trans. Magn. **MAG-22**, 1057 (1986).
[4] S. Sawamura and S. Iwasaki, *et al.*, IEEE Trans. Magn. **MAG-6**, 646 (1970).
[5] S. Chikazumi and S. H. Charap, *et al.*, *Physics of Magnetism* (Wiley, New York, 1984).
[6] A. Winslow, J. Comput. Phys. **1**, 149 (1967).